Development of a charge-transfer distribution model for stack simulation of solid oxide fuel cells

2016 J. Phys.: Conf. Ser. 745 032148

(http://iopscience.iop.org/1742-6596/745/3/032148)

Development of a charge-transfer distribution model for stack simulation of solid oxide fuel cells

H Onaka[1], H Iwai[1], M Kishimoto[1], M Saito[1], H Yoshida[1], G Brus[2] and J S Szmyd[2]

[1]Department of Aeronautics and Astronautics, Kyoto University, Nishikyo-ku, Kyoto, 615-8540, Japan
[2] Department of Fundamental Research in Energy Engineering, AGH-University of Science and Technology, 30 Mickiewicza Avenue, 30-059 Krakow, Poland

E-mail: onaka.hironori.52r@st.kyoto-u.ac.jp

Abstract. An overpotential model for planar solid oxide fuel cells (SOFCs) is developed and applied to a stack numerical simulation. Charge-transfer distribution within the electrodes are approximated using an exponential function, based on which the Ohmic loss and activation overpotential are evaluated. The predicted current-voltage characteristics agree well with the experimental results, and also the overpotentials within the cell can reproduce the results obtained from a numerical analysis where the distribution of the charge-transfer current within the electrodes is fully solved. The proposed model is expected to be useful to maintain the accuracy of SOFC simulations when the cell components, consisting of anode, electrolyte and cathode, are simplified into one layer element.

1. Introduction

Solid oxide fuel cells (SOFCs) are devices that directly convert the chemical energy of fuels into electrical energy through electrochemical reactions, and are attracting attention due to their high power generation efficiency. As the ceramic materials used in SOFCs can exhibit sufficient oxygen ion conductivity only at high temperatures (700-1000°C), the operating temperature of SOFCs is higher than other fuel cell systems. This high temperature improves overall system efficiency by waste heat recovery in cogeneration systems. At the same time, it also promotes degradation of SOFC cells, therefore proper thermal management is required to mitigate thermally induced degradation.

Direct measurements of characteristic variables of operating SOFCs, such as local temperature, concentration and current density, are difficult because of the high operation temperature and narrow channel gaps. Numerical simulation techniques can therefore be used as an effective tool to obtain detailed information inside the SOFCs. Sophisticated numerical models, from electrode scale to stack scale, have been developed and used to analyse the SOFC systems [1]–[4]. In the stack-level modelling, computation cost tends to significantly increase because the computational domain includes not only the cell components but also flow channels and separators. Therefore it is common to simplify the cell component (anode, electrolyte and cathode) into one layer element, called PEN (positive electrode, electrolyte, negative electrode), to reduce the total computation cost [5]. In such approaches, however, the charge-transfer distribution in the electrodes is inevitably neglected, and the Ohmic losses and activation overpotentials may not be estimated correctly.

In this study, we develop a model that evaluates the Ohmic loss and activation overpotential in a PEN element in the stack analyses, based on the approximation of the charge-transfer current

distribution by an exponential function. The model is applied to a stack model and used to predict current-voltage characteristics. The results are compared with the experimental results obtained from a stack experiment, and also with numerical results from a model where the PEN element is fully solved.

2. Numerical model

A coupled multicomponent thermo-fluid and electrochemical model is solved in this study. The thermo-fluid model provides the temperature and species concentration fields in the cell, based on which the electromotive force and overpotentials are calculated and used to obtain of the electric potential field and the electrochemical reaction rate. Velocity and other variables are assumed to be uniformly distributed in the channel height (*y*-) direction, while the distributions in the streamwise (*x*-) and spanwise (*z*-) directions are calculated by solving the governing equations.

2.1. Geometry

Figure 1 shows the schematic of a planar SOFC cell used in the analysis. An anode supported cell consists of Ni-YSZ anode, YSZ electrolyte and LSCF cathode and is considered as single layer element. The fuel and air channels are formed by porous metal to achieve uniform flow field and better current collection. Insulation materials are placed at the upstream and downstream areas of the PEN. The entire structure is sandwiched by metal separators. The size of the cell components (table 1) and the microstructural parameters of the electrodes (table 2) are taken from a stack experiment [6]. The microstructural parameters of the porous metal is shown in table 3 [7].

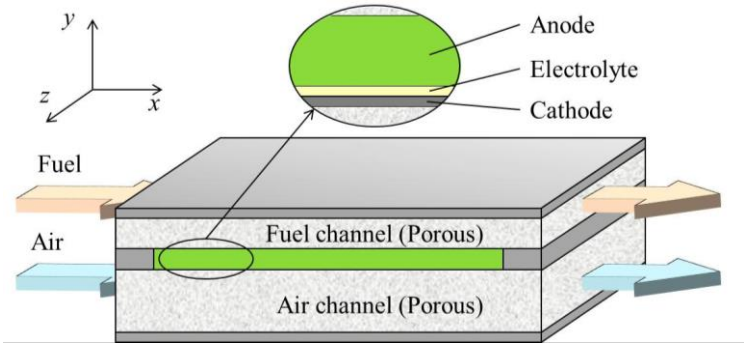

Figure 1. Schematic view of single cell.

Table 1. Cell geometry [mm].

PEN length	PEN width	Channel height (fuel)	Channel height (air)	Electrolyte thickness	Anode thickness	Cathode thickness	Separator thickness
100	100	0.7	1.4	0.008	0.24	0.05	0.2

Table 2. Microstructural parameters of the electrodes.

Parameter	Anode	Cathode	Unit
Volume fraction	Ni: 0.366/ YSZ: 0.383/ Pore: 0.251	LSCF: 0.522/ Pore: 0.478	[-]
Tortuosity factor	Ni: 4.8/ YSZ: 2.4/ Pore: 19.8	LSCF: 2.0/ Pore: 2.0	[-]
TPB density	6.12×10^{12}	-	[m/m^3]
DPB density	-	6.77×10^{6}	[m^2/m^3]

Table 3. Parameters of the porous medium.

Parameter	Value	Unit
Porosity ε	0.9	[-]
Pore diameter d_p	2.0×10^{-4}	[m]
Permeability K	2.0×10^{-9}	[m^2]
Inertia coefficient f	0.046	[-]
Pore specific surface area a_{sf}	1.65×10^{4}	[m^2/m^3]

2.2. Thermo-fluid model

Both fuel and air flows are assumed to be steady and laminar. The heat transfer to the fluid in the porous channel is assumed to occur only through the solid surface of the porous material. Radiative heat transfer within the cell is not taken into account. Physical values, such as velocity, molar fractions and temperature, are locally averaged in a representative elementary volume (REV) [5]. Velocities are averaged within the gas volume in the REV, whereas all the other variables are averaged in the total REV volume. The followings are the transport equations of the averaged physical values in the fluid phase of the porous channels.

Continuity

$$\frac{\partial(\rho u)}{\partial x}+\frac{\partial(\rho w)}{\partial z}=S_k \tag{1}$$

Momentum conservation

$$\begin{aligned}\left[\frac{\partial}{\partial x}\left(\frac{\rho uu}{\varepsilon}\right)+\frac{\partial}{\partial z}\left(\frac{\rho wu}{\varepsilon}\right)\right]&=-\varepsilon\frac{\partial p}{\partial x}+\frac{\partial}{\partial x}\left(\mu\frac{\partial u}{\partial x}\right)+\frac{\partial}{\partial z}\left(\mu\frac{\partial u}{\partial z}\right)\\&+\frac{1}{3}\frac{\partial}{\partial x}\left(\mu\frac{\partial u}{\partial x}\right)-\frac{2}{3}\frac{\partial}{\partial x}\left(\mu\frac{\partial w}{\partial z}\right)+\frac{\partial}{\partial z}\left(\mu\frac{\partial w}{\partial x}\right)-\varepsilon\frac{\mu}{K}u-\varepsilon\frac{\rho f}{\sqrt{K}}|\boldsymbol{v}|u\end{aligned} \tag{2}$$

$$\begin{aligned}\left[\frac{\partial}{\partial x}\left(\frac{\rho uw}{\varepsilon}\right)+\frac{\partial}{\partial z}\left(\frac{\rho ww}{\varepsilon}\right)\right]&=-\varepsilon\frac{\partial p}{\partial z}+\frac{\partial}{\partial x}\left(\mu\frac{\partial w}{\partial x}\right)+\frac{\partial}{\partial z}\left(\mu\frac{\partial w}{\partial z}\right)\\&+\frac{1}{3}\frac{\partial}{\partial z}\left(\mu\frac{\partial w}{\partial z}\right)-\frac{2}{3}\frac{\partial}{\partial z}\left(\mu\frac{\partial u}{\partial x}\right)+\frac{\partial}{\partial x}\left(\mu\frac{\partial u}{\partial z}\right)-\varepsilon\frac{\mu}{K}w-\varepsilon\frac{\rho f}{\sqrt{K}}|\boldsymbol{v}|w\end{aligned} \tag{3}$$

Energy conservation

$$\frac{\partial\left(\rho C_p uT_f\right)}{\partial x}+\frac{\partial\left(\rho C_p wT_f\right)}{\partial z}=\frac{\partial}{\partial x}\left[\lambda_f^{\text{eff}}\frac{\partial T_f}{\partial x}\right]+\frac{\partial}{\partial z}\left[\lambda_f^{\text{eff}}\frac{\partial T_f}{\partial z}\right]+h_{sf}a_{sf}\left(T_s-T_f\right) \tag{4}$$

Mass transfer

$$\frac{\partial}{\partial x}(\rho uY_i)+\frac{\partial}{\partial z}(\rho wY_i)=\frac{\partial}{\partial x}\left(\rho D_{im}\frac{\partial\varepsilon Y_i}{\partial x}\right)+\frac{\partial}{\partial z}\left(\rho D_{im}\frac{\partial\varepsilon Y_i}{\partial z}\right)+S_i \tag{5}$$

The gas properties are dependent on the local temperature and concentration of chemical species in the gas mixture [8]–[13]. ε, K, f, and a_{sf} are the porosity, permeability, inertia coefficient and specific surface area of the porous material, respectively. The third term on the RHS of the equation (4) is the heat exchanged between the fluid phase and the solid phase in the porous material. h_{sf} and λ_f^{eff} are the heat transfer coefficient and effective thermal conductivity, respectively, which are also evaluated using a foam metal assumption [14]. D_{im} is the effective diffusion coefficient. S_k in the continuity equation is associated with the oxygen transfer by the electrochemical reaction. S_i in the mass transfer equation is related to the electrochemical reactions.

The energy equations for the solid phase of the porous channels and the solid plates can be expressed as follows.

$$0=\frac{\partial}{\partial x}\left(\lambda_s^{\text{eff}}\frac{\partial T_s}{\partial x}\right)+\frac{\partial}{\partial z}\left(\lambda_s^{\text{eff}}\frac{\partial T_s}{\partial z}\right)+h_{sf}a_{sf}\left(T_f-T_s\right)+Q \tag{6}$$

$$0=\frac{\partial}{\partial x}\left(\lambda_s\frac{\partial T_s}{\partial x}\right)+\frac{\partial}{\partial z}\left(\lambda_s\frac{\partial T_s}{\partial z}\right)+Q \tag{7}$$

The third term on the RHS of equation (6) corresponds to the heat exchanged between the fluid phase and the solid phase. The effective thermal conductivity λ_s^{eff} is evaluated assuming a foamed metal [14]. The heat generated by Joule heating and the heat conduction in the channel height direction (y direction) are included in the source term Q in these equations. The source term in equation (7) also includes the heat generated from the electrochemical reaction and that associated with the voltage losses in the PEN.

2.3. Electrochemical model

The electromotive force E is locally evaluated using the Nernst equation.

$$E = -\frac{\Delta G_0}{2F} - \frac{RT}{2F}\ln\left[\frac{P_{\mathrm{H_2O}}}{P_{\mathrm{H_2}}\left(P_{\mathrm{O_2}}/101325\right)^{0.5}}\right] \tag{8}$$

The charge-transfer current distribution in the electrodes is assumed with an exponential function [15].

$$i_{\mathrm{ct}}(\xi) = \lambda I e^{-\lambda\xi} \tag{9}$$

where I is the area specific current and $i_{\mathrm{ct}}(\xi)$ is the volumetric density of the local charge-transfer current. The ξ axis is embedded in the electrode with the origin at the electrode-electrolyte interface. λ is the attenuation factor, which determines the thickness of the active reaction area. The determination of the attenuation factor is explained later.

The total activation overpotential in each electrode can be evaluated as follows.

$$\eta_{\mathrm{act}} = \int_0^L \eta_{\mathrm{act,local}}(\xi) i_{\mathrm{ct}}(\xi) d\xi \Big/ \int_0^L i_{\mathrm{ct}}(\xi) d\xi \tag{10}$$

where L is the total thickness of each electrode. The local activation overpotential and the local charge-transfer current are correlated by the Butler-Volmer equation.

$$i_{\mathrm{ct,ano}} = i_{0,\mathrm{ano}} l_{\mathrm{TPB}}\left[\exp\left(\frac{2F}{RT}\eta_{\mathrm{act,local}}\right) - \exp\left(-\frac{F}{RT}\eta_{\mathrm{act,local}}\right)\right] \tag{11}$$

$$i_{\mathrm{ct.cat}} = i_{0,\mathrm{cat}} A_{\mathrm{DPB}}\left[\exp\left(\frac{1.2F}{RT}\eta_{\mathrm{act,local}}\right) - \exp\left(-\frac{F}{RT}\eta_{\mathrm{act,local}}\right)\right] \tag{12}$$

where i_0 is the exchange current per unit TPB length or DPB area [1], [16].

$$i_{0,\mathrm{ano}} = 31.4 P_{\mathrm{H_2}}^{-0.03} P_{\mathrm{H_2O}}^{0.4} \exp\left(-\frac{18300}{T}\right) \tag{13}$$

$$i_{0,\mathrm{cat}} = 1.47\times 10^6 P_{\mathrm{O_2}}^{0.2} \exp\left(-\frac{10327}{T}\right) \tag{14}$$

To analytically obtain the total activation overpotential by equation (10), the equation (11) and (12) need to be explicitly solved in terms of $\eta_{\mathrm{act,local}}$. When $\eta_{\mathrm{act,local}}$ is small, the first-order Taylor expansion (linear approximation) is useful; on the other hand, when $\eta_{\mathrm{act,local}}$ is large enough, the second term is simply ignored (Tafel approximation). However, when $\eta_{\mathrm{act,local}}$ is around 0.1 V, both of these approximation introduces significant errors to the calculation. Therefore, in this study, we proposed a method to approximate the equation (11) using a hyperbolic sine function with a parameter α as follows.

$$i_{\mathrm{ct,ano}} = 2 i_{0,\mathrm{ano}} \sinh\left(\frac{\alpha F}{RT}\eta_{\mathrm{act,local}}\right) \tag{15}$$

Figure 2 shows the relative error in the estimation of the charge-transfer current when the linear approximation, Tafel approximation and hyperbolic sine approximation are used. Note that α is set as 0.05. It is found that the hyperbolic sine approximation can approximate the Butler-Volmer equation with relatively smaller errors in the entire local activation overpotential regime.

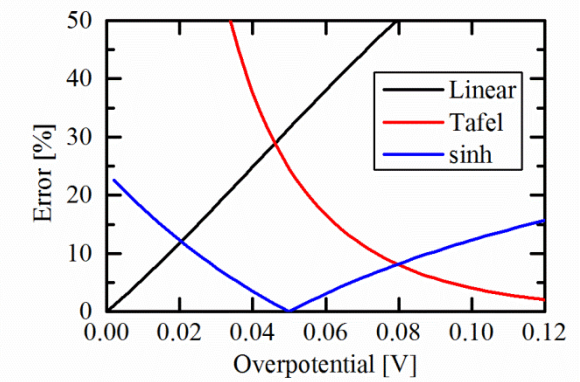

Figure 2. Relative errors in the approximation of the Butler-Volmer equation.

In this study, the hyperbolic sine approximation is employed in the anode, whereas the linear approximation in the cathode.

$$i_{\mathrm{ct,ano}} = 2i_{0,\mathrm{ano}} \sinh\left(\frac{\alpha F}{RT}\eta_{\mathrm{act,local}}\right) \tag{16}$$

$$i_{\mathrm{ct,cat}} = i_{0,\mathrm{cat}} \frac{2.2F}{RT}\eta_{\mathrm{act,local}} \tag{17}$$

By using equation (16) and (17), the total activation overpotential can be expressed as follows.

$$\eta_{\mathrm{act,ano}} = \frac{RT}{\alpha F}\left(\sinh^{-1}\frac{\lambda I}{2i_{\mathrm{ct,ano}}} + \frac{2i_{\mathrm{ct,ano}}}{\lambda I}\left(1 - \sqrt{\left(\frac{\lambda I}{2i_{\mathrm{ct,ano}}}\right)^2 + 1}\right)\right) \tag{18}$$

$$\eta_{\mathrm{act,cat}} = \frac{\lambda RTI}{4.4Fi_{\mathrm{ct,cat}}} \tag{19}$$

The Ohmic losses in each electrode are evaluated as follows using the equation (9).

$$\eta_{\mathrm{ohm}} = \int_0^L \left\{\int_0^\xi \frac{i_{\mathrm{io}}}{\sigma_{\mathrm{io}}^{\mathrm{eff}}} d\xi'\right\} i(\xi) d\xi \Big/ \int_0^L i(\xi) d\xi = \frac{I}{2\lambda\sigma_{\mathrm{io}}^{\mathrm{eff}}} \tag{20}$$

In addition the Ohmic loss in the electrolyte is expressed as follows.

$$\eta_{\mathrm{ohm,ele}} = \frac{I}{\sigma_{\mathrm{io}}} h_{\mathrm{ele}} \tag{21}$$

Concentration overpotential also depends on the charge-transfer current distribution within the electrodes; however, this dependence is neglected in this study because of the fact that the anode is much thicker than the active thickness, and that the cathode concentration overpotential is negligible due to the thin cathode. Thus, the concentration overpotentials are evaluated as follows.

$$\eta_{\mathrm{con,ano}} = -\frac{RT}{2F}\ln\left(\frac{P_{\mathrm{H_2,TPB}} P_{\mathrm{H_2O}}}{P_{\mathrm{H_2}} P_{\mathrm{H_2O,TPB}}}\right) \tag{22}$$

$$\eta_{\mathrm{con,cat}} = -\frac{RT}{4F}\ln\left(\frac{P_{\mathrm{O_2,DPB}}}{P_{\mathrm{O_2}}}\right) \tag{23}$$

where $P_{i,\mathrm{TPB}}$ and $P_{i,\mathrm{DPB}}$ is a partial pressure of gas species i at the electrode-electrolyte interface [17].

$$P_{\mathrm{H_2,TPB}} = P_{\mathrm{H_2}} - \frac{RTL_{\mathrm{ano}}}{2FD_{\mathrm{H_2}}^{\mathrm{eff}}} I, \qquad P_{\mathrm{H_2O,TPB}} = P_{\mathrm{H_2O}} + \frac{RTL_{\mathrm{ano}}}{2FD_{\mathrm{H_2O}}^{\mathrm{eff}}} I \tag{24}$$

$$P_{\mathrm{O_2,TPB}} = P - \left(P - P_{\mathrm{O_2}}\right)\exp\left(\frac{RTL_{\mathrm{cat}}}{4FD_{\mathrm{O_2}}^{\mathrm{eff}} P} I\right) \tag{25}$$

The attenuation factor λ is determined so as to minimize the total overpotential $\eta_{\mathrm{total}} = \eta_{\mathrm{act}} + \eta_{\mathrm{ohm}} + \eta_{\mathrm{con}}$ in the electrodes. Therefore λ is obtained by solving $\partial\eta_{\mathrm{total}}/\partial\lambda = 0$ as follows.

$$\lambda_{\mathrm{ano}} = \frac{2i_{0,\mathrm{ano}}}{I}\sqrt{\left(1 + \frac{\alpha F I^2}{4RT\sigma_{\mathrm{io}}^{\mathrm{eff}} i_{\mathrm{ct,ano}}}\right)^2 - 1} \tag{26}$$

$$\lambda_{\mathrm{cat}} = \sqrt{\frac{2.2Fi_{\mathrm{ct,cat}}}{\sigma_{\mathrm{io}}^{\mathrm{eff}} RT}} \tag{27}$$

The terminal voltage of the PEN at a given current is then determined as follows.

$$V_t = E - \eta_{\mathrm{total,ano}} - \eta_{\mathrm{total,cat}} - \eta_{\mathrm{ohm,ele}} \tag{28}$$

The electric potential in the solid phase is solved using the following equation.

$$\frac{\partial}{\partial x}\left(\sigma_{\mathrm{s}}^{\mathrm{eff}}\frac{\partial V}{\partial x}\right) + \frac{\partial}{\partial z}\left(\sigma_{\mathrm{s}}^{\mathrm{eff}}\frac{\partial V}{\partial z}\right) = S \tag{29}$$

where $\sigma_{\mathrm{s}}^{\mathrm{eff}}$ is the effective electronic conductivity. The source term S is associated with the current from/to the PEN.

3. Results and discussion

3.1. Model validation

The current voltage characteristics obtained from the simulation are shown in figure 3 and compared with the experimental results [6]. The flow and temperature conditions are taken from the stack experiment as shown in table 4. In the model A, the charge-transfer current distribution in the electrodes is approximated using the exponential function, whereas in the model B, the charge-transfer reaction occurs only at the electrode-electrolyte interface. Therefore the Ohmic loss due to the ionic conduction in the electrodes is neglected in the model B. It is found that the model B underestimates the overpotentials in the cell, yielding higher current density under a given terminal voltage. This is mainly because the model B cannot evaluate the contribution of the Ohmic loss in the electrodes. The error between the model B and experiments is larger at lower temperature, because lowering the cell temperature decreases the ionic conductivity of the YSZ phase, increasing the relative contribution of the Ohmic loss to the total overpotential. The model A proposed in this study is found to give better agreement with the experimental results at the both temperature conditions. This clearly emphasizes the benefit of giving more reasonable charge-transfer current distribution within the electrodes. The quantitative discrepancy remaining between the model A and the experiment is considered to be due to the contact resistance between the electrode surface and the current collector, which has not yet been taken into account in this study. For more accurate prediction of the cell performance, the effect of the contact resistance needs to be implemented in the model.

Figure 4 shows comparison of the area-specific resistance (ASR) of the cell obtained at 700 °C at a terminal voltage of 0.9 V. In addition to the model A and B, simulation is also conducted using a model where the distribution of the electrochemical potentials and gas partial pressures are fully solved, and the results are compared with those from the model A and B. It can be also found from this analysis that neglecting the Ohmic loss in the electrodes results in a significant error in the estimation of the total ASR of the cell. The model A gives reasonable estimation not only to the total ASR of the cell but also the breakdown of the ASR components. This clearly indicates the superiority of the proposed PEN model over the conventional PEN model.

Table 4. Input values used in the simulation.

Parameters	Value	Unit
Hydrogen flow rate	1.8	[L min^{-1}]
Nitrogen flow rate	1.2	[L min^{-1}]
Air flow rate	18.0	[L min^{-1}]
Operation temperature	800, 700	[°C]

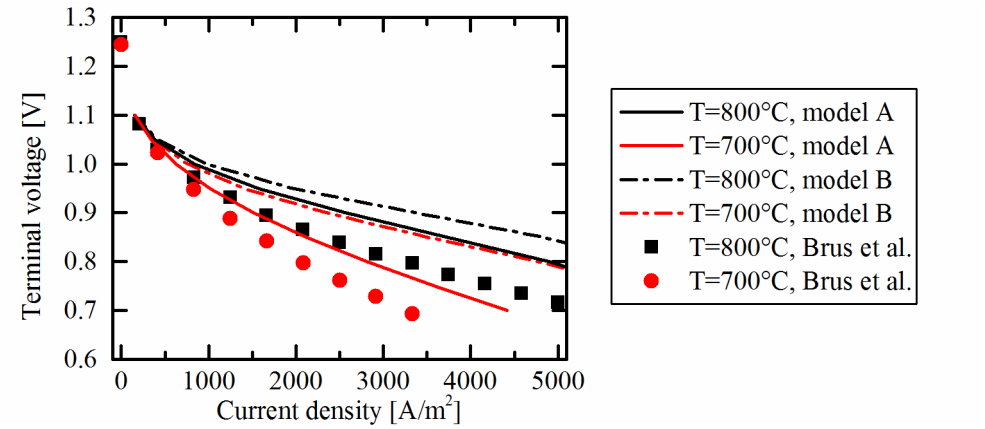

Figure 3. Comparison of model prediction and experimental results [6].

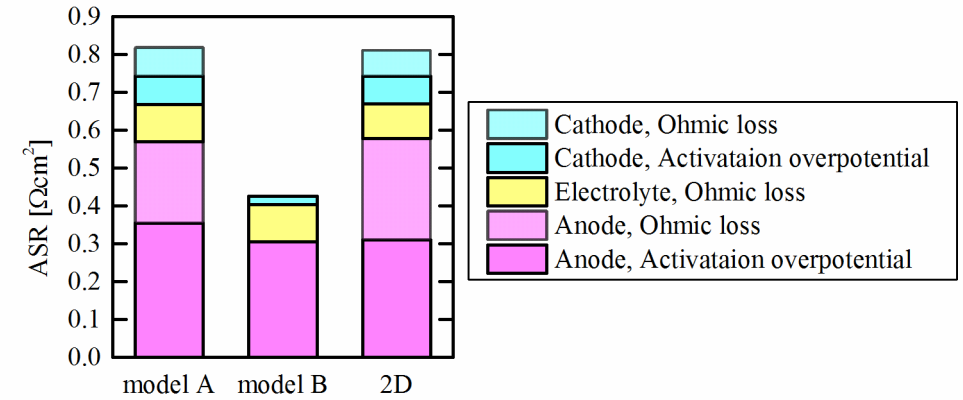

Figure 4. Area specific resistance (ASR) of the PEN at a terminal voltage of 0.9 V at 700 °C.

3.2. Effect on the characteristics

The effects of the different assumption of the charge-transfer distribution on the fundamental characteristics inside the cell are discussed in this section. The inlet gas temperature is 700 °C and the average current density is set at 3000 A/m^2. The thermal insulation boundary conditions are applied to the surface of the cell. Figure 5 shows the local temperature and current density distribution at the center of the cell (z = 0.03). It is found from figure 5(a) that the cell temperature increases along the streamwise direction due to the heat generated from the electrochemical reaction and the voltage losses. The average cell temperature is higher when the model A is used, because the model A considers the Joule heating in the electrodes in addition to the heat associated with the activation and concentration overpotentials. Figure 5(b) clearly shows the difference in the predicted current density distribution from the two models; the model A gives a peak at around x = 0.05 mm, while the model B gives no peak. This is because the total voltage loss is underestimated in the model B and hence the electrochemical reaction can occur from the inlet edge of the electrode. On the contrary, in the model A, the temperature increase found in figure 5(a) gradually decreases the resistance of the cell, enhancing the electrochemical reaction. The decrease trend in the current density in the downstream region is due to the fuel dilution.

It is found that the difference in the assumption of the charge-transfer current distribution in the electrodes affects not only the current-voltage characteristics but also the local temperature and current density distribution inside the cell. When discussing the degradation of the cells caused by temperature gradient and/or fuel starvation, accurate estimation of the charge-transfer current distribution is necessary.

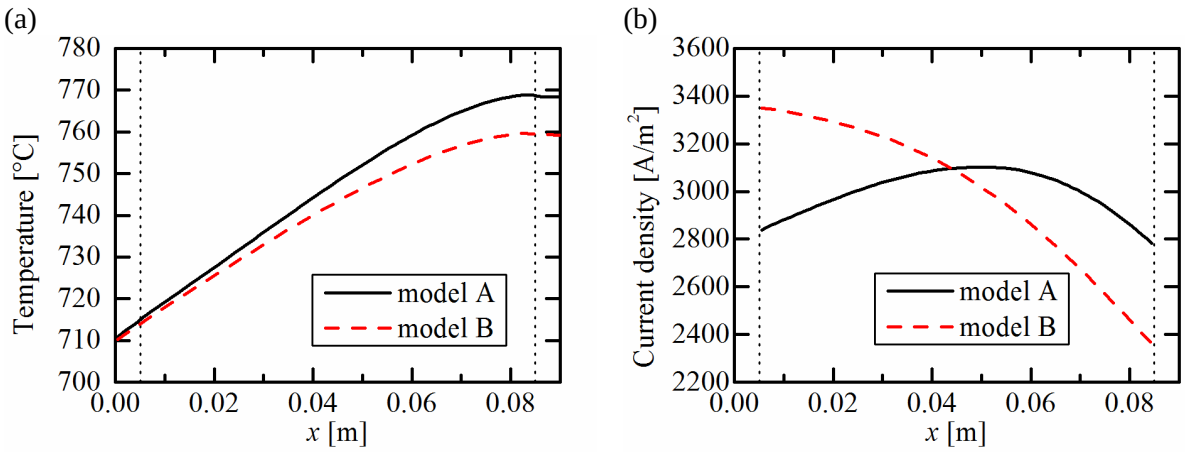

Figure 5. Distributions of the (a) local temperature and (b) local current density with a current density of 3000 A/m^2 at z = 0.03 m.

4. Conclusions

The charge-transfer distribution within the electrodes of SOFCs are approximated using an exponential function, based on which the Ohmic loss and activation overpotential were evaluated. The Butler-Volmer equation is also approximated using a hyperbolic sine function on the anode side and a Taylor series on the cathode side, and the activation overpotential and Ohmic loss in the electrodes are analytically obtained. The predicted current-voltage characteristics gives better agreement with the experimental results, and also the overpotentials within the cell can reproduce the results obtained from a numerical analysis where the distribution of the charge-transfer current within the electrodes are fully solved. However, predicted performance still overestimated due to the effect of contact resistance between the electrodes and separators, which has not yet been considered in the present study. Implementation of a contact resistance model is required for further improving the model accuracy, and is one of the further works. The proposed model is expected to be useful to maintain the accuracy of SOFC simulations when the cell components are simplified into single layer PEN element.

Acknowledgements

This present work was partially supported by the PAN-JSPS Joint Research Project “Mechanism behind degradation in SOFCs – from nano to macro-scale” and partially by the New Energy and Industrial Technology Development Organization (NEDO).

References

[1] Matsuzaki K, Shikazono N and Kasagi N 2011 *J. Power Sources* **196** 3073–82
[2] Ackmann T, de Haart L G J, Lehnert W and Stolten D 2003 *J. Electrochem. Soc.* **150** A783–9
[3] Janardhanan V M and Deutschmann O 2007 *Chem. Eng. Sci.* **62** 5473–86
[4] Severson H and Assadi M 2011 *J. Fuel Cell Sci. Tech.* **8** 051021-1–13
[5] Iwai H, Yamamoto Y, Saito M and Yoshida H 2011 *Energy* **36** 2225–34
[6] Brus G, Iwai H, Sciazko A, Saito M, Yoshida H and Szmyd J S 2015 *J. Power Sources* **288** 199–205
[7] Bhattacharya A, Calmidi V V and Mahajan R L 2002 *Int. J. Heat Mass Transfer* **45** 1017–31
[8] Incropera F P and Dewitt D P 1996 *Introduction to Heat Transfer 3rd Edition* (John Wiley & Sons)
[9] Bird R B, Stewart W E and Lightfoot E N 2002 *Transport Phenomena 2nd Edition* (John Wiley & Sons)
[10] Bromley L A and Wilke C R 1951 *Ind. Eng. Chem.* **43** 1641–48
[11] Wilke C R 1950 *Chem. Eng. Prog.* **46** 95–101
[12] Fuller E N, Schettler P D and Giddings J C 1966 *Ind. Eng. Chem.* **58** 19–27
[13] Lindsay A L and Bromley L A 1950 *Ind. Eng. Chem.* **42** 1508–11
[14] Calmidi V V and Mahajan R L 1999 *J. Heat Transfer* **121** 466–71
[15] Miyawaki K, Kishimoto M, Iwai H, Saito M and Yoshida H 2014 *J. Power Sources* **267** 503–14
[16] de Boer B 1998 *Ph.D. Thesis* (University of Twente, The Netherland)
[17] Chan S H, Khor K A and Xia Z T 2001 *J. Power Sources* **93** 130–40